Chemical Engineering Journal 338 (2018) 82–91

Contents lists available at ScienceDirect

Chemical Engineering Journal

journal homepage: www.elsevier.com/locate/cej

Morphology controlled porous poly(lactic acid)/zeolitic imidazolate framework-8 fibrous membranes with superior PM2.5 capture capacity

Xiu Dai, Xu Li, Xinlong Wang*

School of Chemical Engineering, Nanjing University of Science & Technology, Nanjing 210094, China

HIGHLIGHTS

- Porous structure PLA/ZIF-8 fibrous membranes were prepared.
- The PLA/ZIF-8 membranes showed superior PM2.5 capture efficiency.
- The process and mechanism of PM2.5 capture were studied.

ARTICLE INFO

Keywords:
Poly(lactic acid)
ZIF-8
Porous structure
PM2.5 capture
Barrier property

ABSTRACT

In this work, the nanoparticles of zeolitic imidazolate framework-8 (ZIF-8) are incorporated into poly (lactic acid) (PLA) to prepare porous electrospun membranes. The morphology, mechanical property as well as the PM capture process and capacity of the membranes are studied using scanning electron microscopy (SEM), BET test, X-ray diffraction (XRD), tensile test, Fourier infrared spectra (FT-IR), UV–visible spectra, thermogravimetric analyses (TGA) and photoelectron spectroscope (XPS), systematically. The results demonstrate that the diameter and nanoscale porous structure of fibres can be successfully controlled by changing the content ZIF-8. The PLA/ZIF-8 membranes show better mechanical property compared with pure PLA membrane. The PM capture measurement demonstrates that the PLA/ZIF-8 porous membranes exhibit significantly enhanced PM2.5 removal efficiency compared to that of the pure PLA membrane. The prepared porous membranes also show low pressure drops and good recycling performance.

1. Introduction

Suspended particulate matter (PM), which is a complex mixture of extremely small solid particles and moisture, has been considered one of the most serious environmental issues [1–3]. On the basis of size, PM can be classed into two types as PM10 and PM2.5, representing particle sizes below 10 and 2.5 μm, respectively [4]. Long-term exposure to PM2.5 has been consistently associated with lung cancer [5,6], cerebrovascular disease [7], neurodegeneration [8], etc. People use various air filters to prevent inhaling PM in haze. However, most of those air filters have shortcoming of poor PM2.5 rejection.

Polymer fibrous membranes made by electrospinning have great advantages of high surface area, good air permeability and good internal connectivity, making them good candidates as air filters. What's more, the morphology of the electrospun fibre which is vital in blocking and adsorbing fine particles from air can be controlled by changing the parameters of electrospinning or/and by modification [9,10]. The Group of Cui demonstrated that the electrospun polymer nanofibers (i.e., polyacrylonitrile (PAN), polyimide (PI), and nylon-6 (PA6)) had strong affinity to PM pollutants and therefore showed a high removal efficiency at low pressure drop and a high optical transparency [11–13]. Jing et al. modified the electrospun PAN using ionic liquid diethylammonium dihydrogen phosphate (DEAP) for PM2.5 removal. The modified PAN nanofibers exhibited significantly improved PM2.5 capture capacity compared to that of the pure PAN nanofibers [14]. Compared with those mentioned polymers, poly(lactic acid) (PLA), which is produced from renewable resources and biodegradable, is more environmentally friendly [15,16]. Wang et al. fabricated various porous bead-on-string PLA nanofibrous membranes by regulating the solution concentration and the ratio of the solvent mixture [17]. They found filtration efficiency and pressure drop for the resultant PLA membranes could be controlled by modifying the morphology of the fibres. They also prepared hybrid PLA/TiO_2 fibrous membranes via the electrospinning technique. They found the PLA/TiO_2 fibrous membranes exhibiting excellent air filtration performance and good antibacterial activity [18].

* Corresponding author.
E-mail address: wxlong@njust.edu.cn (X. Wang).

https://doi.org/10.1016/j.cej.2018.01.025
Received 9 November 2017; Received in revised form 4 January 2018; Accepted 4 January 2018
Available online 05 January 2018
1385-8947/

Metal-organic frameworks (MOFs), as one of the emerging porous crystalline materials, are composed of metal ions linked together by organic bridging ligands [19]. Adding MOFs into a polymer matrix to fabricate MOFs based composites has been intensively studied in recent years [20,21]. The MOFs/polymer composites are potentially applied in gas storage [22], microencapsulation [23], catalysis [24], and separation [25]. Recently, MOFs have shown excellent potential for application in air purification due to their large surface areas as well as rich functionalities [26–28]. Combining porous fibres with porous MOFs will be a new method for designing and modifying the structure of filter media to improve filtration performance. However, study on the PM2.5 capture capacity of the PLA/MOFs electrospun membranes has not been reported.

In this study, we have explored the possibility of fabricating high efficient PM2.5 capture electrospun membranes with improved performance by incorporating zeolitic imidazolate framework-8 (ZIF-8, $Zn(MeIm)_2$, MeIm = 2-methylimidazole) with PLA matrix. ZIF-8 is one of the most important primary members of MOFs. Its structure analogous to zeolites that are built upon 4-connected nets of tetrahedral units, wherein Zn^{2+} is linked through N atoms in imidazolate anions [29]. The crystal structure of ZIF-8 is shown in Scheme 1. Its highly accessible pores, great surface area, high thermal stability, chemical stability and long-term stability in gas atmosphere make it a good candidate for air purification [27,30–32]. Therefore, we introduced the ZIF-8 nanoparticles into PLA matrix to fabricate porous nanocomposite membranes. The surface morphology, mechanical properties and adsorption capacity for PM2.5 of the porous composite fibres have been systematically studied.

2. Experimental section

2.1. Materials

Poly(lactic acid) (Haizheng 290, melt flow index of 10–30 g/10 min) was obtained from Zhejiang Hai Zheng Biological Materials Co. Ltd, China. 2-Methylimidazole (98%) was purchased from Aladdin Industrial Corporation. $Zn(NO_3)_2{\cdot}6H_2O$, methanol (99.5%) and CH_2Cl_2 (99.5%) were obtained from Sinopharm Chemical Reagent Co. Ltd, China.

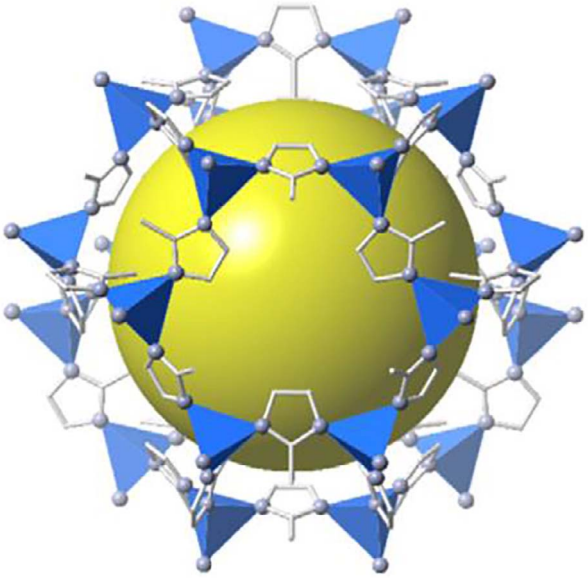

Scheme 1. Crystal structure of ZIF-8: Zn (polyhedral), N (sphere), and C (line) [33]

2.2. Synthesis of ZIF-8

The ZIF-8 nanoparticles were synthesized in a manner similar to a previously reported procedure [34]. At first, 5 mmol of $Zn(NO_3)_2{\cdot}6H_2O$ was dissolved in 100 mL of methanol. Subsequently, 20 mmol of 2-methylimidazole was dissolved in 100 mL of methanol. Two solutions were mixed thoroughly under stirring with a magnetic bar for 1 h. After standing for 12 h, the resultant particles were centrifuged and washed with fresh methanol and then dried at 80 °C.

2.3. Preparation of the porous PLA/ZIF-8 fibrous membranes

For the preparation of PLA/ZIF-8 samples, different loadings of ZIF-8 (0, 1, 2, 3, 5 wt% based on the weight of PLA) were dispersed in 10 mL CH_2Cl_2 by an ultrasonic mixing for 30 min. Then, the PLA pellets (10 wt%) were dissolved in the ZIF-8 suspension by stirring at room temperature. The mixture was stirred for 4 h to obtain uniform composite solution before being loaded in a 10 mL syringe. The electrospinning process as shown in Scheme 2 proceeded under 22 kV voltage and 0.5 mL/h feeding rate. A metal screen collector covered with copper screen was centered vertically at a distance of 20 cm from the syringe tip. The porous PLA/ZIF-8 fibrous membranes with thickness of ~0.1 mm (measured by a digital display micrometer) were compiled to form a mat for further characterization. For brevity, the samples containing 0, 1, 2, 3 and 5 wt% ZIF-8 are abbreviated as PLA, PZD1, PZD2, PZD3 and PZD5 from now on.

2.4. Characterization techniques

The morphology of PLA/ZIF-8 porous fibrous membranes was investigated by a Hitaclhi S-4800 scanning electron microscopy (SEM, Hitachi, Japan). The specific surface area (SSA) of PLA and PLA/ZIF-8 membranes were determined from the N_2 isotherm adsorption at 77.5 K recorded on an ASAP2020 BET surface analyzer (Micromeritics, America). Prior to the adsorption measurements, the samples were degassed for 8 h at 323.15 K. X-ray diffraction (XRD) measurements were carried out by a D8 Advance diffractometer (Bruker, Germany) at 40 kV and 40 mA with Cu Ka radiation (λ = 0.15418 nm). The Fourier infrared spectra (FT-IR) ranging from 400 to 4000 cm^{-1} were obtained by FT-IR-8400S spectrometer (Shimadzu, Japan) with the resolution of 2 cm^{-1}. Changes in the UV–visible spectra on the samples were monitored with a UV-2101PC spectrophotometer (Shimadzu, Japan). Tensile testing was performed on a CMT tensile tester (Sans, China) with a rate of 10 mm/min at room temperature. The samples with known thickness were cut into strip with dimensions of 0.5 cm × 4 cm. The values were averaged over five measurements. Thermogravimetric analyses (TGA) were performed using a TGA/SDTA851e (Shimadzu, Japan). The samples were heated from 30 to 600 °C with a heating rate of 20 °C/min under nitrogen flow. The bonding information of the samples before and after adsorption were analysed by a PHI 5300 X-ray photoelectron spectroscope (XPS, PE, America).

2.5. PM adsorption measurement

The PM was generated by burning cigarette. The inflow concentration was controlled by diluting the smoke using moist air to a hazardous pollution level equivalent to the PM2.5 index > 800 $\mu g/m^3$. The mixture of PM and moisture was introduced into a glass container at a flow rate of 1.5 L/min. The samples covered on the top of the container. The smoke system was refreshed every 5 min to keep the high concentration of PM2.5 during the 60 min measurement. A LD-5/5J particle counter (TLYE, China) was used to detected PM particle concentration. The pressure drop was measured by an EM201B differential pressure gauge (UEi, American).

In order to investigate the recycling performance of the PLA/ZIF-8 membranes. PZD2 after 60 min adsorption was ultrasonic cleaned in

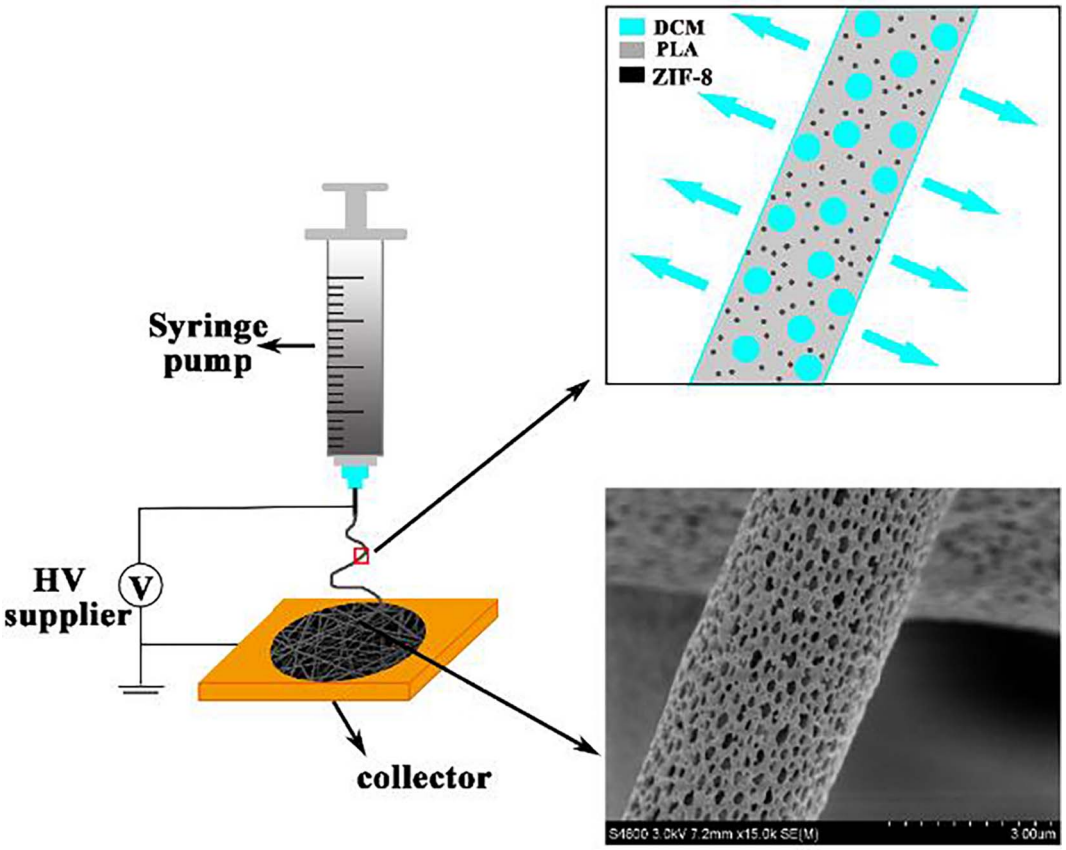

Scheme 2. The schematic diagram electrospinning of the PLA/ZIF-8 porous nanofibers.

70% (v/v) ethanol/water for 1 min. The washed membranes were put on a piece of glass and dried at 50 °C. Then, the PM removal efficiency and the pressure drop were measured.

3. Results and discussion

3.1. Morphology of the PLA/ZIF-8 fibrous membranes

The morphology of the PLA/ZIF-8 fibrous membranes was investigated by SEM. SEM micrographs and diameter distributions (analyzed by Nano Measurer 1.2) of the porous PLA/ZIF-8 fibrous membranes are shown in Fig. 1. Our previous work has proven that the addition of the ZIF-8 nanoparticles can adjust the diameter of PLA fibres [35]. Fig. 1 shows as the incorporation of ZIF-8 nanoparticles, the diameter is decreased, and the diameter distribution becomes narrow, which is consistent with what we reported. The decrease of the diameter can be attributed to the fact that the addition of the ZIF-8 nanoparticles reduces the surface energy [36,37]. Besides, the incorporation of the ZIF-8 nanoparticles can increase the stability of the PLA/ZIF-8 solution and thus narrows the diameter distribution [38]. The combination of SEM and the image processor software Image J2 has been proved to be a powerful tool for analysis of the porous materials [39,40]. The high magnification SEM images of the prepared membranes are analyzed by Image J2 to estimate the average pore size, pore area fraction and perimeter of pores. As shown in Table 1, the average pore size, pore area fraction and perimeter of pores increase significantly in presence of ZIF-8. The average pore size, pore area fraction and pores perimeter increase from 0.018 μm^2, 20.7% and 0.53 μm for pure PLA to 0.080 μm^2, 35.7% and 1.09 μm for PZD2, respectively. The pore area fraction of PZD2 is higher than that of the hierarchical structured nano-sized/porous poly(lactic acid) (PLA-N/PLA-P) composite fibrous membrane, which shows great air filtration performance [41].The addition of the ZIF-8 nanoparticles to the PLA matrix results in more and larger pores appearing, suggesting that ZIF-8 particles promote the formation of pores on the fibre surface. The BET SSA of the porous membranes are also shown in Table 1. It is obvious that adding ZIF-8 increases the specific surface, which is helpful for the capture of PM2.5. There are not any agglomerations can be seen on the surface of PLA/ZIF-8 porous fibre due to the good dispersion of ZIF-8 in the PLA matrix.

3.2. The XRD of the PLA/ZIF-8 fibrous membranes

Fig. 2 shows the XRD patterns of pure ZIF-8, pure PLA fibrous membranes and the PLA/ZIF-8 fibrous membranes with different ZIF-8 content. As shown in Fig. 2(a), there is an exceptionally wide diffraction from 10° to 25° for all membrane samples, which is caused by the scattering of the PLA matrix [42]. The sharp peak around 7.41°, which is attributed to the reflections of the plane of ZIF-8, appears in XRD patterns of the PLA/ZIF-8 fibrous membranes, indicating the presence of ZIF-8 on the surface of the porous PLA fibres. However, after the 60 min PM adsorption, the (1 1 0) diffraction peak of PZDs disappears or becomes weak, suggesting that the ZIF-8 nanoparticles can adsorb PM onto their surface.

3.3. The mechanical property of the PLA/ZIF-8 membranes

The mechanical property is always one of the most important indexes to make use of membranes reasonably and effectively. The typical stress-strain curves and the values of the tensile strength and strain at break are shown in Fig. 3. It can be seen in Fig. 3 that the stress-strain curves of the porous PLA/ZIF-8 membranes are similar to other unaligned electrospun membranes [43]. With the increasing content of ZIF-8, the values of the tensile strength and the strain at break show a

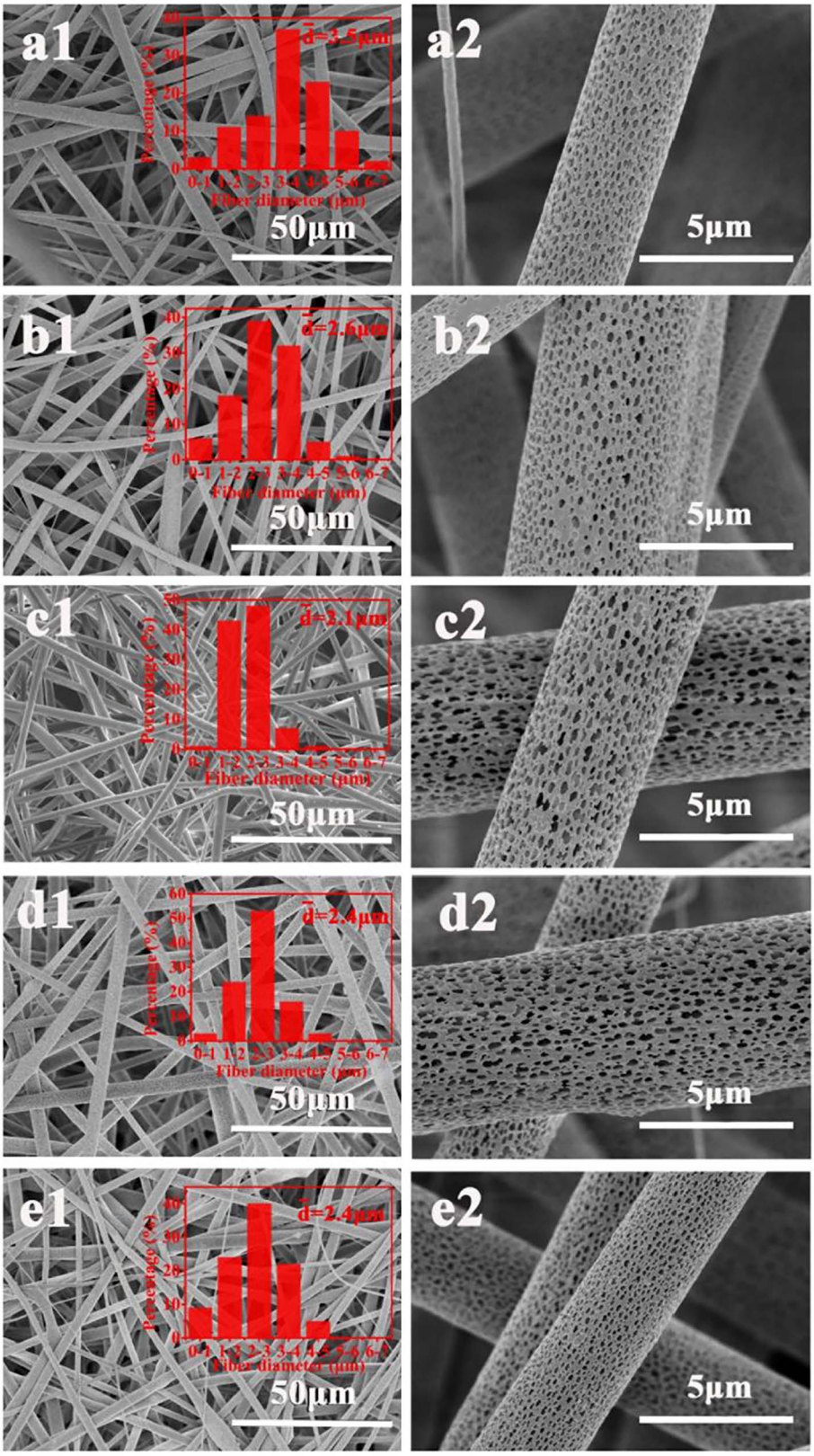

Fig. 1. The SEM of PLA/ZIF-8 fibrous membranes before PM adsorption measurement (a1, a2: PLA; b1, b2: PZD1; c1, c2: PZD2, d1, d2: PZD3, e1, e2: PZD5.)

nonmonotonic trend, reaching the maximum when ZIF-8 content is 2 wt %. However, PLA with 0.5 wt% ZIF-8 is the optimized formulation in our previous work. The difference may be caused by the different fabricating parameters. In case of PZD2, the tensile strength (2.86 MPa) is more than twice that of the pure PLA membrane (1.26 MPa). The tensile strength of PZD2 is not as high as the PLA/ZIF-8 dense nanofiber (3.44–5.02 MPa) due to the porous structure [35]. The strain at break increases from 56.6% for PLA to 100.5% for PZD2. The increase in tensile strength and strain at break indicate an efficient load transfer from the PLA matrix to the ZIF-8 particles. The efficient load transfer

Table 1
Average pore size, area fraction, perimeter of pores and BET SSA of PLA and PLA/ZIF-8 membranes.

Sample	Average pore size (μm^2)	Pore area fraction (%)	Perimeter (μm)	BET SSA (m^2/g)
PLA	0.018 ± 0.002	20.7 ± 0.7	0.53 ± 0.07	19.80
PZD1	0.031 ± 0.001	25.5 ± 0.1	0.60 ± 0.01	22.31
PZD2	0.080 ± 0.001	35.7 ± 0.5	1.09 ± 0.02	25.24
PZD3	0.079 ± 0.001	31.5 ± 0.4	1.09 ± 0.02	25.16
PZD5	0.041 ± 0.003	29.1 ± 0.2	0.81 ± 0.03	23.75

could be attributed to the good dispersion of ZIF-8 in the matrix and the good interfacial adhesion between the PLA matrix and the ZIF-8 nanoparticles.

3.4. The PM capture property of the PLA/ZIF-8 membranes

The thermogravimetric (TG) test was performed to evaluate the adsorption capacity of the PLA and ZIF-8/PLA porous membranes. The TG curves of all samples before and after PM adsorption are displayed in Fig. 4(a) and Fig. S1. As shown in Fig. 4(a) and Fig. S1, the TG curve for each sample changes a lot after PM adsorption. Before PM capture, all samples show one thermal degradation stage which mainly caused by the degradation of PLA matrix. However, there are three thermal degradation stages after PM capture. It is apparent that the first and the third weight loss stages completely result from the adsorbed PM. The significant weight loss at the second stage is mainly caused by the bare sample. Briefly, take the PLA as sample (Fig. 4(a)), we evaluated the PM adsorption capacity by dividing the sum of the weight losses in the first (9.23%) and third (7.10%) stages by the second-stage (83.63%) weight loss. As shown in Fig. 4(b), the calculated capacity of PLA, PZD1, PZD2, PZD3 and PZD5 are 19.5%, 29.5%, 35.5%, 34.6% and 28.6%, respectively. Jing et al. [14] reported that DEAP-modified PAN nanofibers exhibited significantly enhanced PM2.5 capture capacity. They also evaluated the PM2.5 adsorption capacity by TG test, and their maximum PM2.5 capture capacity is only 21.9%. The presence of ZIF-8 nanoparticles significantly increases the PM adsorption capacity of the porous membranes. There are three possible reasons for the increase of adsorption efficiency. Firstly, the reduction in fibre diameter can enhance the adsorption property [44]. Furthermore, the porous structure of ZIF-8 provides more sites for PM2.5 capture and enhances the interaction between the composite and PM2.5 [27]. Finally, the interaction between the membranes and PM can be strengthen by the functional groups and open metal sites.

The removal efficiency was calculated by the following equation:

$$\text{Removal efficiency} = (1-C/C_0) \times 100\% \quad (1)$$

Where C_0 and C are the PM concentrations before and after passing through the membrane when adsorbed for 5 min, respectively. As shown in Fig. 5(a), PLA, PZD1, PZD2, PZD3 and PZD5 achieve PM2.5 and PM10 removal efficiencies of 85.49%, 88.63%, 94.61% 94.41%, 94.44% and 90.53%, 91.58%, 94.82%, 97.90%, 96.57%, respectively. The porous PLA/ZIF-8 membranes show higher removal efficiencies for PM, especially for PM2.5, than the neat PLA membrane. The PM removal efficiencies of PZD2 at different capture time are shown in Fig. 5(b). In 60 min adsorption process, PZD2 achieves PM2.5 and PM10 removal efficiencies of 92.33–96.81% and 94.82–98.75%, respectively. Besides the efficiency, a low air flow resistance is also an important performance for the filtration membranes. The pressure drops of PLA membranes with different ZIF-8 content are shown in Fig. 5(a). At a face velocity of 12.5 cm/s, the pressure drops of all samples are less than 50 Pa. The pressure drops of PLA/ZIF-8 membranes are lower than that of neat PLA, which may result from the higher porosity of the PLA/ZIF-8 membranes.

In addition, the recycling performance of PZD2 was evaluated. After 60 min adsorption, PZD2 was washed in 70% ethanol by sonication. The washed and dried membrane was used again to capture PM. As shown in Fig. 6, after three cycles, the removal efficiency for PM2.5 and PM10 decreases slightly and remain higher than 88%. The pressure drop increases with the increasing of used times and remain lower than 80 Pa. Xiong et al. speculated that the increase of pressure drop is due to the residual particles which lead to increased air resistance [45].

In order to understand the PM capture process, the morphology of PZD2 with different time of PM capture was examined by SEM. As shown in Fig. 7, lots of pores randomly distribute on the surface of PZD2 fibres before PM capture. After 10 min adsorption of PM, some deposits are observed, filling part of pores. The high porous structure of PZD2 fibre provides many attachment points for PM. It is obvious that the size of the particles adsorbed by the pores on the surface of PLA fibre is smaller than 2.5 μm, suggesting that the porous PLA/ZIF-8 membranes can capture PM2.5 effectively More deposits are observed after 20 min capture and the pores on the surface of fibres are obviously decreased, suggesting that more PM2.5 are adsorbed. After 60 min capture of PM, the smoke PM formed a coating layer tightly wrapped around the PZD2 fibres.

The Fourier infrared spectra and UV–vis spectra of PZD2 before and after 60 min PM capture are shown in Fig. 8. The principal absorbance peaks obtained for PZD2 are as follows: (i) the strong peak at 1730 cm^{-1} is attributed to the C=O stretching, (ii) the peaks at 1443 cm^{-1} and 1347 cm^{-1} are attributed to the C–H bending vibration, (iii) the peaks around 1175 cm^{-1} and 1069 cm^{-1} are assigned to the symmetric and asymmetric mode of C–O–C stretching, respectively, (iv) the peak at 862 cm^{-1} is due to the C–COO stretching [46,47]. After the adsorption of PM, the spectrum of PZD2 is changed. The peaks at 1730 cm^{-1}, 1175 cm^{-1} and 1069 cm^{-1} shift to

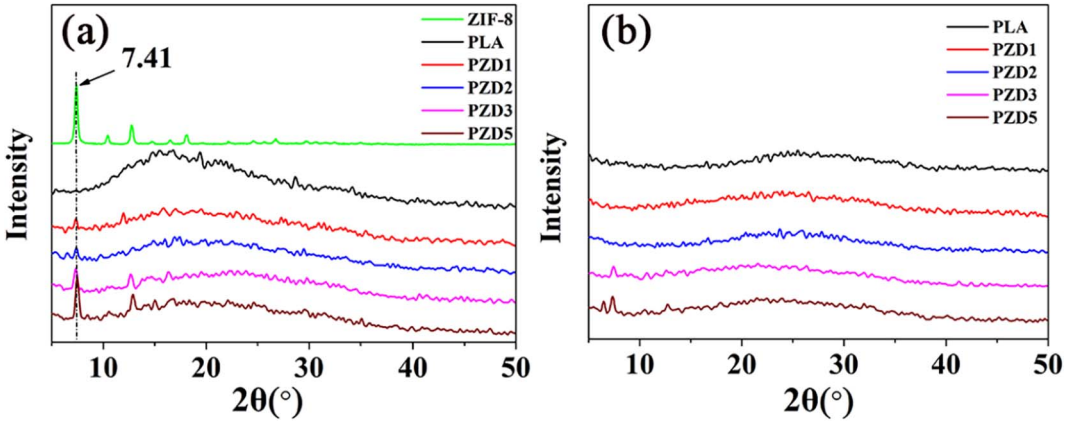

Fig. 2. The XRD pattern of ZIF-8 nanoparticles and the PLA/ZIF-8 porous membranes before (a) and after PM capture (b).

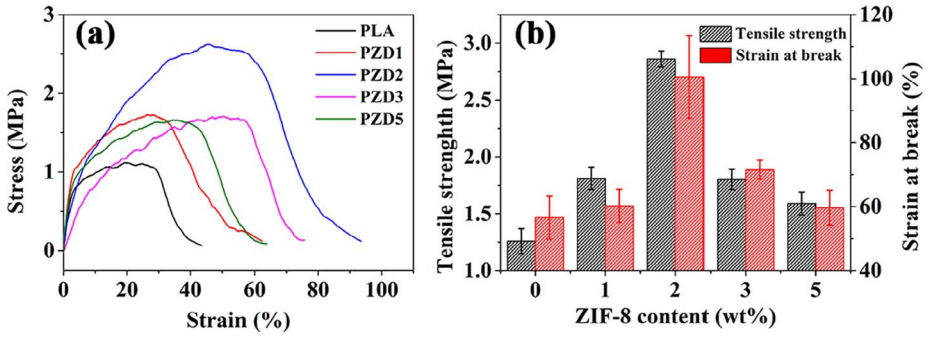

Fig. 3. (a) The stress-strain curves and (b) the values of the tensile strength and strain at break.

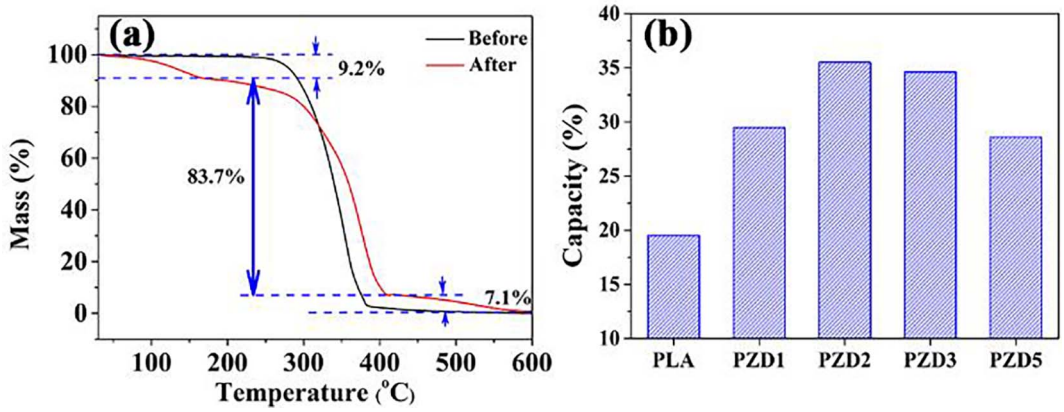

Fig. 4. (a) TG analyses of PLA before and after 60 min of PM2.5 capture, (b) the PM2.5 adsorption capacity of PLA and its composites.

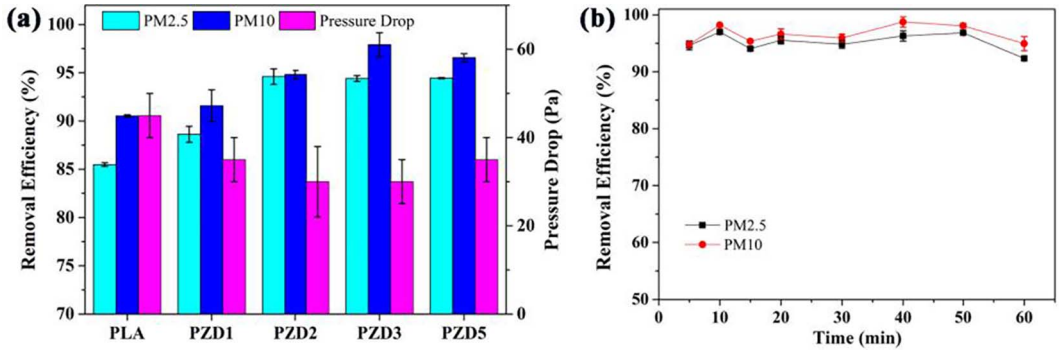

Fig. 5. (a) PM2.5 and PM10 removal efficiencies of PLA and PLA/ZIF-8 porous membranes, (b) PM2.5 and PM10 removal efficiencies of PZD2 at different capture time.

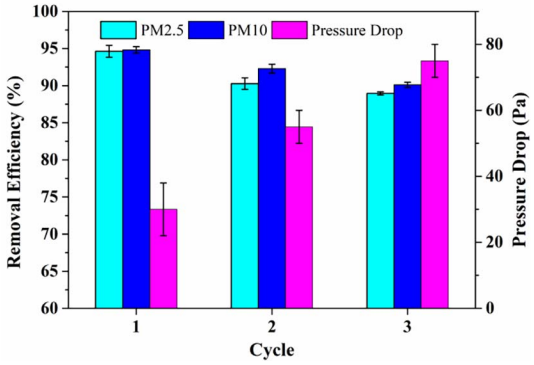

Fig. 6. PM2.5 and PM10 removal efficiencies and the pressure drop of PZD2 after different recycling tests.

1743 cm^{-1}, 1179 cm^{-1} and 1081 cm^{-1}, respectively. Additionally, a new peak at 841 cm^{-1} appears in the spectrum. The shifting of main peaks to higher wavenumber and the appearance of new peak suggests the existence of great interactions between PZD2 fibres and PM., Before PM capture, PZD2 only shows one peak at 210 nm in Fig. 8(b). After 60 min PM capture, the peak at 210 nm shifts to 213 nm, suggesting the interactions between PZD2 and PM. Additionally, a new peak at 267 nm appears, which can be attributed to the nicotine produced by burning cigarettes [48].

In the experiment of PM adsorption, one side of the membrane is the air with PM (A-side) and another is clean air (B-side). Fig. 9 shows the photos of the two sides of PZD2 membrane with different PM capture time. As time goes on, the color of A-side is changed gradually from white to tan indicating increased PM capture. However, the color of B-side does not change with time, suggesting that the PLA/ZIF porous membrane has good PM barrier performance.

X-ray photoelectron spectroscope (XPS) was performed to investigate the composition of PZD2 before and after (two sides) PM capture. Fig. 10 shows the XPS characterization of PZD2 before and after 10 min PM capture. The main composition of PZD2 before and after (two sides) 10 min PM capture is listed in Table 2. As shown in Fig. 10, C1s spectra of untreated PZD2 comprise three major peaks at

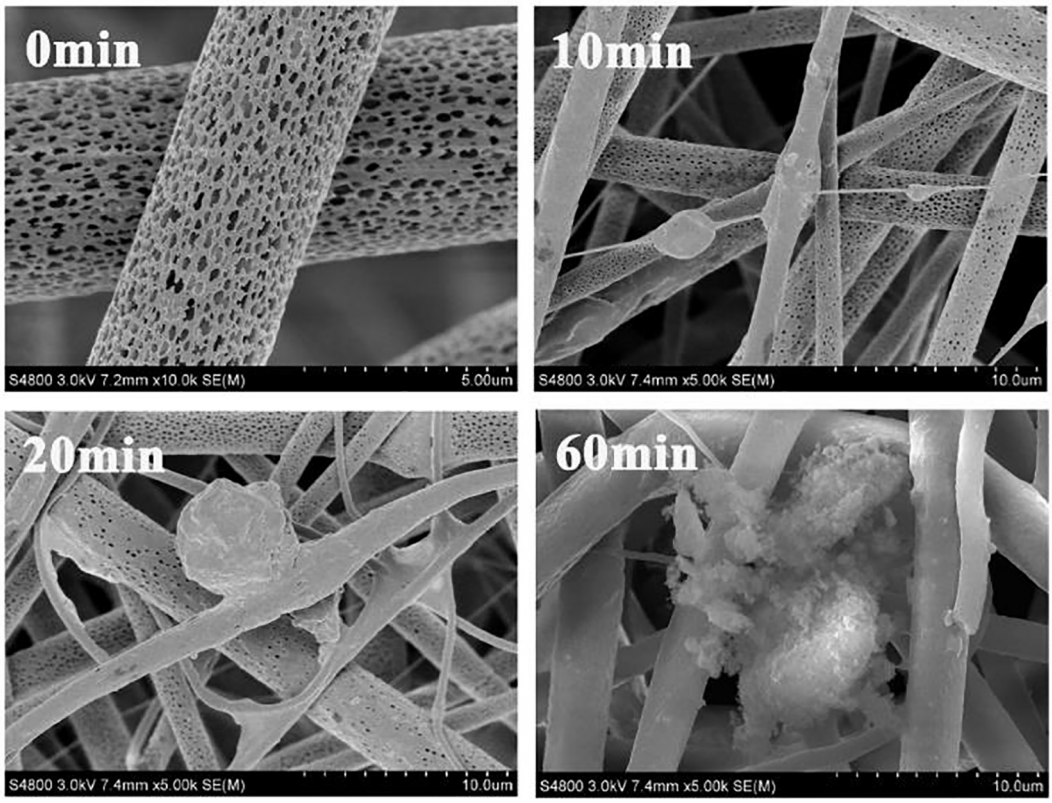

Fig. 7. SEM images of PZD2 with different time of PM capture.

284.6 eV, 286.5 eV and 288.6 eV, corresponding to C—C/C—H bonds, C—O—C group and C═O group, respectively [49]. Since the content of N is very low, there is not any peak that can be seen in N1s spectra of untreated PZD2. It can be seen in Table 2 that the contents of C, O and N of untreated PZD2 are 60.9%, 38.8% and 0.3%, respectively. As shown in Fig. 9, after 10 min PM capture, only a small amount of PM is captured. However, remarkable changes can be found from the C1s signal of A-side. The peak at around 288.6 eV is significantly decreased compared to that of the untreated PZD2, indicating the decrease in the amount of C═O group. The N1s signal of A-side appears at 399.0 eV, which is attributed to the C—N bond from PM [11]. The contents of C, O, N and Zn of A-side are 75.2%, 22.5% and 1.7%, respectively. It is obvious that the presence of PM significantly changes the composition of the membranes surface. The C1s and N1s spectra of B-side are almost as same as that of untreated PZD2 and the composition of B-side is very close to that of untreated PZD2, suggesting that there is almost no PM on the surface B-side. The results of XPS further confirm the perfect barrier property of PZD2.

The proposed PM capture mechanism of the porous PLA/ZIF-8 electrospun membrane is shown in Fig. 11. The large size PM, which cannot even go through the gaps between fibres, can be easily blocked by the membrane. The PM in smaller size, such as PM2.5, can be captured by the large number of pores on the surface of PLA fibres. In presence of ZIF-8, the interaction between the composite and PM is strengthen due to the functional groups and open metal sites. Apart from the functional groups and open metal sites, the ZIF-8 nanoparticles on the surface of PLA fibres can provide more adsorption sites, resulting in the enhanced PM2.5 capture capacity.

4. Conclusion

The porous PLA/ZIF-8 electrospun membranes were prepared successfully. ZIF-8 nanoparticles are uniformly distributed on the surface of porous PLA fibres. The prepared PLA/ZIF-8 membrane with 2 wt%

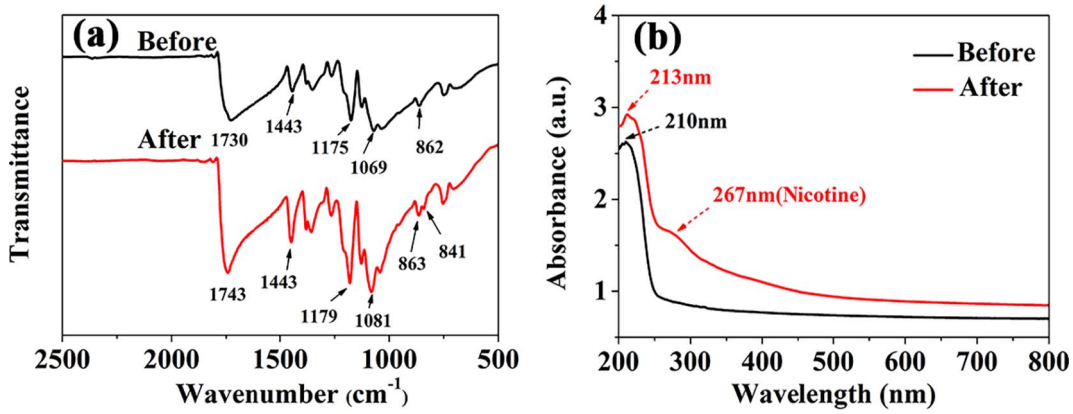

Fig. 8. (a) The FTIR spectra and (b) the UV–vis spectra of the PZD2 before and after the 60 min PM capture.

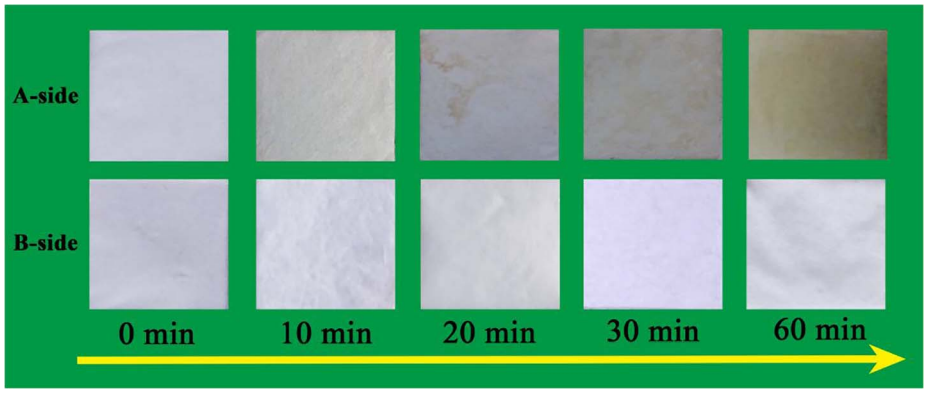

Fig. 9. Photos of PZD2 with different PM capture time.

ZIF-8 shows significantly improved tensile strength and the strain at break compared with pure PLA membrane. When the content of ZIF-8 rises to 5 wt%, the tensile strength and the strain at break of PLA/ZIF-8 membrane do not decrease compared to that of the pure PLA membrane. The PLA/ZIF-8 membrane show great PM2.5 capture efficiency due to the presence of the pores and ZIF-8 particles on the surface of fibres. Moreover, the prepared membranes have low pressure drops and good recycling performance. Owning these unique characters, the porous PLA/ZIF-8 electrospun membranes could be a good candidate as air filter for PM2.5 capture.

Table 2
Composition of PZD2 before and after the 10 min PM capture.

Samples	Composition (%)			
	C	O	N	Zn
PZD2 before PM capture	60.8	38.9	0.3	0.2
PZD2 after PM capture (A-side)	75.2	22.5	1.7	0.1
PZD2 after PM capture (B-side)	62.1	37.4	0.3	0.2

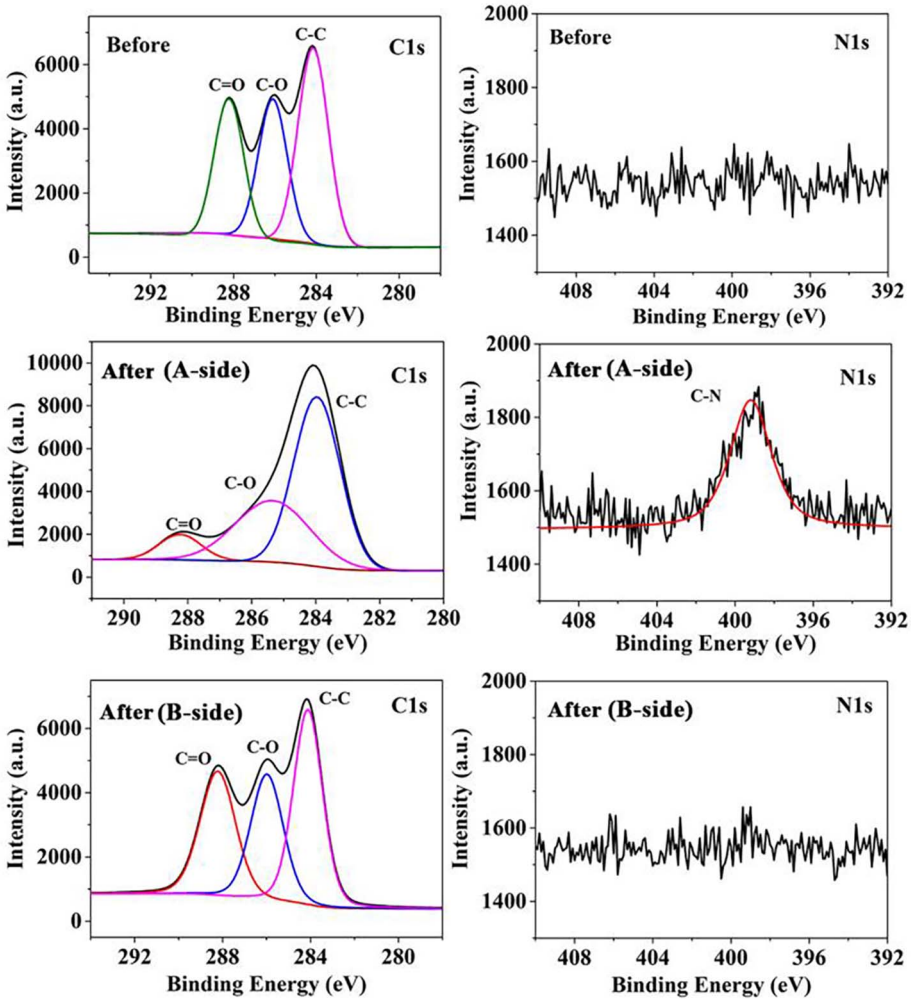

Fig. 10. XPS characterization of PZD2 before and after the 10 min PM capture illustrating C1s and N1s peak analysis.

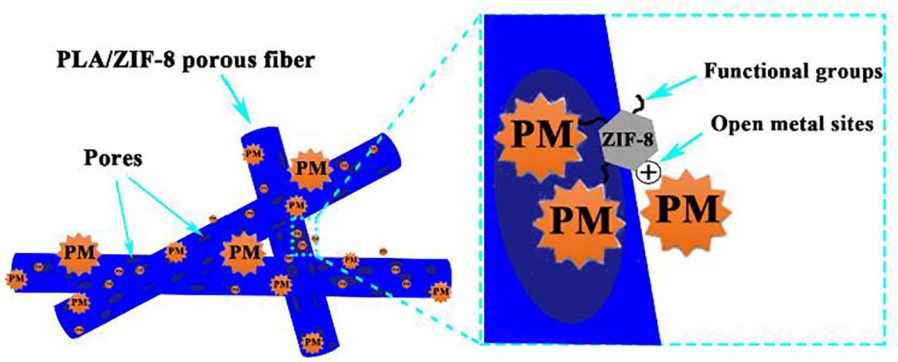

Fig. 11. Proposed capture mechanism of the porous PLA/ZIF-8 electrospun membrane for PM.

Acknowledgements

This work was supported by Science and Technology Support Program (Social Development) of Jiangsu Province of China (BE 2013714) and Priority Academic Program Development of Jiangsu Higher Education Institutions (PAPD).

Appendix A. Supplementary data

Supplementary data associated with this article can be found, in the online version, at http://dx.doi.org/10.1016/j.cej.2018.01.025.

References

[1] N. Fann, A.D. Lamson, S.C. Anenberg, K. Wesson, D. Risley, B.J. Hubbell, Estimating the national public health burden associated with exposure to ambient PM2.5 and ozone, Risk Anal. 32 (2012) 81–95.
[2] S.M. Oh, H.R. Kim, Y.J. Park, S.Y. Lee, K.H. Chung, Organic extracts of urban air pollution particulate matter (PM2.5)-induced genotoxicity and oxidative stress in human lung bronchial epithelial cells (BEAS-2B cells), Mutat. Res. Genet. Toxicol. Environ. Mutagen. 723 (2011) 142–151.
[3] A.P. Tai, L.J. Mickley, D.J. Jacob, Correlations between fine particulate matter (PM 2.5) and meteorological variables in the United States: implications for the sensitivity of PM 2.5 to climate change, Atmos. Environ. 44 (2010) 3976–3984.
[4] J.R. Brook, T.F. Dann, R.T. Burnett, The relationship among TSP, PM10, PM2.5, and inorganic constituents of atmospheric participate matter at multiple Canadian locations, J. Air Waste Manage. 47 (1997) 2–19.
[5] R.T. Burnett, C.A. Pope III, M. Ezzati, C. Olives, S.S. Lim, S. Mehta, H.H. Shin, G. Singh, B. Hubbell, M. Brauer, An integrated risk function for estimating the global burden of disease attributable to ambient fine particulate matter exposure, Environ. Health Perspect. 122 (2014) 397.
[6] G.B. Hamra, N. Guha, A. Cohen, F. Laden, O. Raaschou-Nielsen, J.M. Samet, P. Vineis, F. Forastiere, P. Saldiva, T. Yorifuji, Outdoor particulate matter exposure and lung cancer: a systematic review and meta-analysis, Environ. Health Perspect. 122 (2014) 906.
[7] R. Beelen, M. Stafoggia, O. Raaschou-Nielsen, Z.J. Andersen, W.W. Xun, K. Katsouyanni, K. Dimakopoulou, B. Brunekreef, G. Weinmayr, B. Hoffmann, Long-term exposure to air pollution and cardiovascular mortality: an analysis of 22 European cohorts, Epidemiology 25 (2014) 368–378.
[8] M.-A. Kioumourtzoglou, J.D. Schwartz, M.G. Weisskopf, S.J. Melly, Y. Wang, F. Dominici, A. Zanobetti, Long-term PM2.5 exposure and neurological hospital admissions in the northeastern United States, Environ. Health Perspect. 124 (2016) 23.
[9] A. Vanangamudi, S. Hamzah, G. Singh, Synthesis of hybrid hydrophobic composite air filtration membranes for antibacterial activity and chemical detoxification with high particulate filtration efficiency (PFE), Chem. Eng. J. 260 (2015) 801–808.
[10] H. Katepalli, M. Bikshapathi, C.S. Sharma, N. Verma, A. Sharma, Synthesis of hierarchical fabrics by electrospinning of PAN nanofibers on activated carbon microfibers for environmental remediation applications, Chem. Eng. J. 171 (2011) 1194–1200.
[11] C. Liu, P.-C. Hsu, H.-W. Lee, M. Ye, G. Zheng, N. Liu, W. Li, Y. Cui, Transparent air filter for high-efficiency PM2.5 capture, Nat. Commun. 6 (2015) 6205.
[12] J. Xu, C. Liu, P.-C. Hsu, K. Liu, R. Zhang, Y. Liu, Y. Cui, Roll-to-roll transfer of electrospun nanofiber film for high-efficiency transparent air filter, Nano Lett. 16 (2016) 1270–1275.
[13] B. Khalid, X. Bai, H. Wei, Y. Huang, H. Wu, Y. Cui, Direct blow-spinning of nanofibers on a window screen for highly efficient PM2.5 removal, Nano Lett. 17 (2017) 1140–1148.
[14] L. Jing, K. Shim, C.Y. Toe, T. Fang, C. Zhao, R. Amal, K.-N. Sun, J.H. Kim, Y.H. Ng, Electrospun polyacrylonitrile–ionic liquid nanofibers for superior PM2.5 capture capacity, ACS Appl. Mater. Interfaces 8 (2016) 7030–7036.
[15] X. Wu, Y. Ma, G. Zhang, Y. Chu, J. Du, Y. Zhang, Z. Li, Y. Duan, Z. Fan, J. Huang, Thermally stable, biocompatible, and flexible organic field-effect transistors and their application in temperature sensing arrays for artificial skin, Adv. Funct. Mater. 25 (2015) 2138–2146.
[16] S. Sinha Ray, Polylactide-based bionanocomposites: a promising class of hybrid materials, Acc. Chem. Res. 45 (2012) 1710–1720.
[17] Z. Wang, C. Zhao, Z. Pan, Porous bead-on-string poly (lactic acid) fibrous membranes for air filtration, J. Colloid Interface Sci. 441 (2015) 121–129.
[18] Z. Wang, Z. Pan, J. Wang, R. Zhao, A novel hierarchical structured poly (lactic acid)/titania fibrous membrane with excellent antibacterial activity and air filtration performance, J. Nanomater. 2016 (2016) 39.
[19] S.L. James, Metal-organic frameworks, Chem. Soc. Rev. 32 (2003) 276–288.
[20] Q.-L. Zhu, Q. Xu, Metal–organic framework composites, Chem. Soc. Rev. 43 (2014) 5468–5512.
[21] J. Quirós, K. Boltes, S. Aguado, R.G. de Villoria, J.J. Vilatela, R. Rosal, Antimicrobial metal–organic frameworks incorporated into electrospun fibers, Chem. Eng. J. 262 (2015) 189–197.
[22] E.V. Perez, K.J. Balkus, J.P. Ferraris, I.H. Musselman, Mixed-matrix membranes containing MOF-5 for gas separations, J. Membr. Sci. 328 (2009) 165–173.
[23] J. Huo, M. Marcello, A. Garai, D. Bradshaw, MOF-polymer composite microcapsules derived from pickering emulsions, Adv. Mater. 25 (2013) 2717–2722.
[24] P.C. Sahoo, N.S. Sambudi, S.B. Park, J.H. Lee, J.-I. Han, Immobilization of carbonic anhydrase on modified electrospun poly (lactic acid) membranes: quest for optimum biocatalytic performance, Catal. Lett. 145 (2015) 519–526.
[25] S. Basu, A. Cano-Odena, I.F. Vankelecom, MOF-containing mixed-matrix membranes for CO_2/CH_4 and CO_2/N_2 binary gas mixture separations, Sep. Purif. Technol. 81 (2011) 31–40.
[26] J.B. DeCoste, G.W. Peterson, Metal–organic frameworks for air purification of toxic chemicals, Chem. Rev. 114 (2014) 5695–5727.
[27] Y. Zhang, S. Yuan, X. Feng, H. Li, J. Zhou, B. Wang, Preparation of nanofibrous metal-organic framework filters for efficient air pollution control, J. Am. Chem. Soc. 138 (2016) 5785–5788.
[28] H. Jasuja, G.W. Peterson, J.B. Decoste, M.A. Browe, K.S. Walton, Evaluation of MOFs for air purification and air quality control applications: ammonia removal from air, Chem. Eng. Sci. 124 (2015) 118–124.
[29] Y.R. Lee, M.S. Jang, H.Y. Cho, H.J. Kwon, S. Kim, W.S. Ahn, ZIF-8: a comparison of synthesis methods, Chem. Eng. J. 271 (2015) 276–280.
[30] D. Liu, X. Ma, H. Xi, Y.S. Lin, Gas transport properties and propylene/propane separation characteristics of ZIF-8 membranes, J. Membr. Sci. 451 (2014) 85–93.
[31] H.-S. Choi, S.-J. Lee, Y.-S. Bae, S.-J. Choung, S.H. Im, J. Kim, Scalable continuous solvo-jet process for ZIF-8 nanoparticles, Chem. Eng. J. 266 (2015) 56–63.
[32] K. Tao, C. Kong, L. Chen, High performance ZIF-8 molecular sieve membrane on hollow ceramic fiber via crystallizing-rubbing seed deposition, Chem. Eng. J. 220 (2013) 1–5.
[33] R. Banerjee, A. Phan, B. Wang, C. Knobler, H. Furukawa, M. O'Keeffe, O.M. Yaghi, High-throughput synthesis of zeolitic imidazolate frameworks and application to CO2 capture, Science 319 (2008) 939–943.
[34] J. Cravillon, R. Nayuk, S. Springer, A. Feldhoff, K. Huber, M. Wiebcke, Controlling zeolitic imidazolate framework nano-and microcrystal formation: insight into crystal growth by time-resolved in situ static light scattering, Chem. Mater. 23 (2011) 2130–2141.
[35] X. Dai, Y. Cao, X. Shi, X. Wang, The PLA/ZIF-8 nanocomposite membranes: the diameter and surface roughness adjustment by ZIF-8 nanoparticles, high wettability, improved mechanical property, and efficient oil/water separation, Adv. Mater. Interface 3 (2016) 1600725.
[36] M.F. Haase, K.J. Stebe, D. Lee, Continuous fabrication of hierarchical and asymmetric Bijel microparticles, fibers, and membranes by solvent transfer-induced phase separation (STRIPS), Adv. Mater. 27 (2015) 7013–7013.
[37] C.J. Thompson, G.G. Chase, A.L. Yarin, D.H. Reneker, Effects of parameters on nanofiber diameter determined from electrospinning model, Polymer 48 (2007) 6913–6922.
[38] J.Y. Kim, S.H. Kim, S.W. Kang, J.H. Chang, S.H. Ahn, Crystallization and melting behavior of silica nanoparticles and poly(ethylene 2,6-naphthalate) hybrid nanocomposites, Macromol. Res. 14 (2006) 146–154.
[39] L.F. Pires, F.S. Borges, S. Passoni, A.B. Pereira, Soil pore characterization using free software and a portable optical microscope, Pedosphere 23 (2013) 503–510.
[40] O. Agboola, T. Mokrani, R. Sadiku, Porous and fractal analysis on the permeability

of nanofiltration membranes for the removal of metal ions, J. Mater. Sci. 51 (2016) 2499–2511.
[41] Z. Wang, Z. Pan, Preparation of hierarchical structured nano-sized/porous poly (lactic acid) composite fibrous membranes for air filtration, Appl. Surf. Sci. 356 (2015) 1168–1179.
[42] B.W. Chieng, N.A. Ibrahim, W.M.Z.W. Yunus, M.Z. Hussein, Y.Y. Then, Y.Y. Loo, Effects of graphene nanoplatelets and reduced graphene oxide on poly (lactic acid) and plasticized poly (lactic acid): a comparative study, Polymers 6 (2014) 2232–2246.
[43] Q. Shi, C. Zhou, Y. Yue, W. Guo, Y. Wu, Q. Wu, Mechanical properties and in vitro degradation of electrospun bio-nanocomposite mats from PLA and cellulose nanocrystals, Carbohydr. Polym. 90 (2012) 301–308.
[44] Q. Li, Y. Xu, H. Wei, X. Wang, An electrospun polycarbonate nanofibrous membrane for high efficiency particulate matter filtration, RSC Adv. 6 (2016) 65275–65281.
[45] Z.C. Xiong, R.L. Yang, Y.J. Zhu, F.F. Chen, L.Y. Dong, Flexible hydroxyapatite ultralong nanowire-based paper for highly efficient and multifunctional air filtration, J. Mater. Chem. A 5 (2017) 17482–17491.
[46] D.K. Wang, S. Varanasi, P.M. Fredericks, D.J. Hill, A.L. Symons, A.K. Whittaker, F. Rasoul, FT-IR characterization and hydrolysis of PLA-PEG-PLA based copolyester hydrogels with short PLA segments and a cytocompatibility study, J. Polym. Sci. Poly. Chem. 51 (2013) 5163–5176.
[47] M.A. Sawpan, K.L. Pickering, A. Fernyhough, Effect of fibre treatments on interfacial shear strength of hemp fibre reinforced polylactide and unsaturated polyester composites, Compos. Part A Appl. Sci. 42 (2011) 1189–1196.
[48] P.M. Clayton, C.A. Vas, T. Bui, A.F. Drake, K. McAdam, Spectroscopic studies on nicotine and nornicotine in the UV region, Chirality 25 (2013) 288–293.
[49] H. Shi, Q. Gan, X. Liu, Y. Ma, J. Hu, Y. Yuan, C. Liu, Poly (glycerol sebacate)-modified polylactic acid scaffolds with improved hydrophilicity, mechanical strength and bioactivity for bone tissue regeneration, RSC Adv. 5 (2015) 79703–79714.